XI ECCOMAS Thematic Conference on Smart Structures and Materials
SMART 2025
M. Krommer, M. Nader and M. Schagerl (Eds)

Received: 8 April 2025 / Revised: 1 July 2025 / Accepted: 15 July 2025

MAGNETOMETER-BASED PARTICLE FILTER WITH ENHANCED VELOCITY INPUT FOR GPS-INDEPENDENT NAVIGATION OF UAV

D. PISARSKI, R. FARAJ, R. KONOWROCKI, B. POPŁAWSKI AND Ł. JANKOWSKI

Institute of Fundamental Technological Research (IPPT PAN)
Polish Academy of Sciences
Pawińskiego 5B, 02-106 Warsaw, Poland
e-mail: dpisar@ippt.pan.pl, web page: http://www.ippt.pan.pl/

Abstract. The contribution presents an original method for accurate positioning of an unmanned aerial vehicle (UAV) operating in GPS-denied environment, where GNSS signals may be jammed or spoofed. The proposed approach uses Particle Filtering with an enhanced velocity propagation model to estimate the UAV's position within a magnetic anomaly field. The velocity is estimated based on data fusion of kinematic measurements from an Inertial Measurement Unit (IMU) and magnetic field readings from a scalar magnetometer, which are compared with a magnetic anomaly map. Magnetic field measurements are incorporated at two stages. First, the rate of change of the magnetic field along the UAV's trajectory is introduced into the propagation model using the Bayesian inference to fuse IMU and magnetometer data for a more accurate velocity estimation. Second, measured magnetic field values are compared with the anomaly map to recalculate the particle weights and refine the position estimate. The proposed method was validated using in-flight data. The UAV positioning error was significantly reduced. The results confirm the effectiveness of the proposed and emphasize the high performance of the Particle Filter with enhanced velocity propagation model compared to traditional dead reckoning navigation.

Key words: Magnetic Anomaly Navigation, Unmanned Aerial Vehicle, Particle Filter, Sensor Fusion, Bayesian Inference

1 INTRODUCTION

The accuracy of GNSS-based navigation is degraded in environments with limited or intermittent access to GNSS signal, such as tunnels and dense urban areas. Additionally, GNSS navigation becomes impossible in cases of intentional jamming or spoofing. The need for robust solutions and countermeasures is particularly critical in UAV navigation, where encoders commonly used in robotics cannot be applied, and traditional dead reckoning based on inertial measurements is insufficient. Many types of approaches were developed to ensure reliable navigation under these conditions.

A common method is real-time analysis of terrain features, implemented in vision-based navigation systems. These systems offer relatively high spatial accuracy, which makes them a popular alternative to inertial navigation systems (INS) [1, 2]. However, vision-based methods struggle or fail in environments with few reference points or no reference points at all. This includes navigation over flat deserts, water reservoirs, or dense forests. Additionally, even if vision-based are cost-effective in terms of hardware elements, they face significant limitations related to high computational demands, dependency on lighting conditions, reduced accuracy at high flight altitudes, and vulnerability to common adverse weather conditions such as rain, fog, dust, and snow [3].

As an alternative to vision-based systems, some of recently developed navigation approaches employ measurements of crustal anomalies of the Earth's magnetic field. These magnetic anomalies exhibit significant variability across most environments, including over open water and other visually uniform terrains. This variability and insensitivity to weather conditions makes them a reliable reference for positioning. Furthermore, commercially available magnetic sensors are lightweight and compact, which makes them well-suited for integration into ultralight UAV platforms in hardware terms.

Various techniques and methods have been developed for magnetic positioning, dependent on the characteristics of the intended deployment environment. For indoor applications, SLAM (Simultaneous Localization and Mapping) techniques are commonly applied. Intended for robotic applications, they aim to map the ambient magnetic field, while simultaneously positioning the robot within the mapped environment [4]. To effectively fuse inertial and magnetometric data, SLAM techniques often rely on Particle Filtering [5] or Kalman filters [6]. The feasibility of these approaches has been demonstrated in numerous publications. For example, an extended Kalman filter was used in [7] to reduce noise in measurements of magnetic field gradient for positioning of a foot-mounted IMU/magnetometric system. In [8], an extended Kalman filter was used to fuse data coming from a magnetometer and an IMU installed on a ship model and in a foot-mounted sensor. In [9], a magnetic map-matching algorithm based on sequential batch fusion was proposed for stable and fast indoor localization. In [10], a Bayesian data fusion algorithm was developed for improving the positioning accuracy based on IMU data and magnetometric measurements. Besides indoor implementations, researchers have also extensively explored magnetic anomaly-based navigation systems for outdoor environments, particularly airborne systems. In [11, 12], an airborne magnetic anomaly navigation was developed. For accurate measurements of the magnetic field, scalar sensors are often used. The position drift, typical for navigation systems based on inertial data only, is usually addressed using map-matching techniques. Accuracies within tens of meters were achieved for over hour-long flights [13]. More recently, machine learning techniques have been successfully applied for in-flight navigation based on magnetic anomalies [14].

This contribution considers magnetic anomaly-based navigation intended for aerial applications. Particle Filter is used as a well-established core methodology for positioning. The original element proposed here is the velocity-enhanced propagation model used within the Particle Filter. Unlike traditional approaches relying solely on IMU-based velocity, the proposed method integrates onboard magnetometric measurements and fuses them with inertial data using Bayesian inference to enhance velocity estimation. Below, the general architecture of the system is introduced, followed by the basic mathematical formulas. Thereupon, the proposed method is validated using in-flight data collected with a Vertical Take-off and Landing (VTOL) platform and a scalar magnetometer on-board, tested in an autonomous flight over a designated water area.

2 SYSTEM ARCHITECTURE

UAV position is estimated using an approach based on Particle Filter. The measured magnetic field values, the IMU-provided inertial measurements, and the magnetic anomaly map are used as an input. A general scheme of the system architecture is presented in Fig. 1. Measurements of the magnetic field are utilized twice during the Particle Filter procedure:

1. At the particle re-sampling stage, magnetometer readings are compared with the map of magnetic anomalies, and only particles more aligned with the actual measurements are retained. This is a typical use of magnetometric measurements in magnetic navigation.

2. At the particle propagation stage, magnetometric measurements are used to correct the IMU-based velocity. This fusion of magnetic and inertial data is performed based on Bayesian inference within the block "Velocity Estimation Module" in Fig. 1, and the result is an enhanced particle propagation model. This is the actual novelty of the presented approach.

The related formal mathematical formulas are discussed in the subsequent section. The following assumptions are necessary to ensure the proper operation of the proposed system:

- the velocity drift estimated based on IMU alone is sufficiently small,
- a sufficiently accurate map of magnetic anomalies is available,
- the magnetic anomaly field is sufficiently smooth (continuous spatial derivatives),
- the magnetic anomaly field does not change in time,
- the magnetometric measurements are of a sufficient accuracy to reliably estimate the time derivative of the magnetic anomaly field.

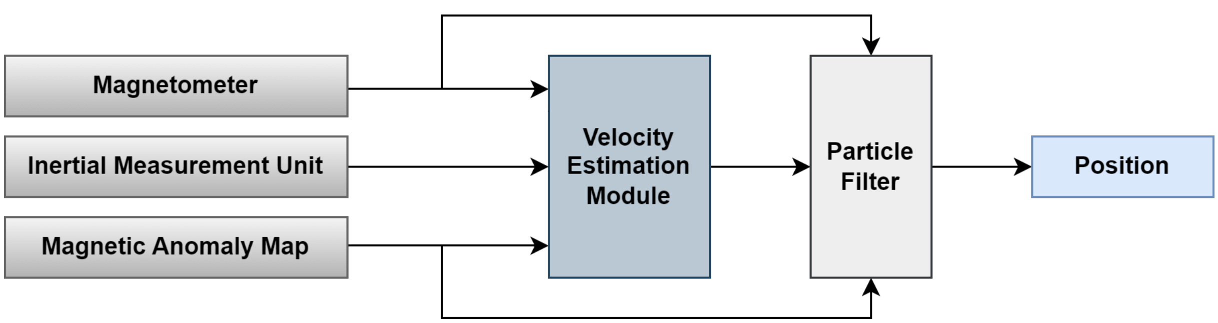

Figure 1: Architecture of the proposed positioning system based on Particle Filter and magnetic anomaly measurements.

3 Particle Filter based on inertial/magnetic data fusion

3.1 Particle Filter procedure

The Particle Filter is a widely used procedure. The distribution p of state X_t at time t is iteratively estimated based on the observation o_t:

$$p(X_t|o_t) = \sum_{i=1}^{N_t} w_t^i \, \delta(X_t - \mathbf{x}_t^i), \tag{1}$$

where N_t is the number of particles at time t, δ is the Dirac delta function, $\mathbf{x}_t^1, ..., \mathbf{x}_t^{N_t}$ are particle locations, and $w_t^1, ..., w_t^{N_t}$ represent their weights. In typical implementations, the the distribution $p(X_t|o_t)$ is computed in the three following steps:

Step 1: Compute the weights w_t^i, $i = 1, ..., N_t$, which should be proportional to the measurement likelihood $p(o_t|X_t)$.

Step 2: Re-sample the particles: discard the particles with lower significance and generate new particles based on the measurement likelihood $p(o_t|X_t)$.

Step 3: Update particle positions to time $t+1$ based on the propagation model.

3.2 Propagation model and velocity correction based on magnetometric measurements

In applications to positioning systems, the state X_t represents the position, and in the system considered here, the observation o_t is the measured magnetic field. Step 3 makes involves the propagation model, and the propagation model requires estimated velocity of the UAV. The velocity is usually obtained by integrating IMU-sourced acceleration and thus susceptible to substantial drift in time. In the propagation model proposed here, velocity $\mathbf{V}_t$ is modeled probabilistically as a 2D Gaussian random variable, and its IMU-based estimation is corrected using magnetometric measurements and Bayesian framework. Step 3 consists of two updates (position and velocity), and it is performed in the three following substeps:

Step 3.1: (*Position update*) The particle location is updated using the expected value of the velocity in the current time step, $\boldsymbol{\mu}_{\mathbf{V}_t} = \mathbb{E}[\mathbf{V}_t]$:

$$\mathbf{x}_{t+1} = \mathbf{x}_t + \Delta t \, \boldsymbol{\mu}_{\mathbf{V}_t},$$

where Δt is the time increment. This formula corresponds to the Euler's numerical integration scheme, and it allows the location update to be decoupled from the velocity update.

Step 3.2: (*Initial velocity correction*) The last-step velocity $\mathbf{V}_t$ is shifted by the velocity update $\Delta\mathbf{V}_{t+1}^{\mathrm{IMU}}$ provided by the IMU to obtain $\bar{\mathbf{V}}_{t+1} = \mathbf{V}_t + \Delta\mathbf{V}_{t+1}^{\mathrm{IMU}}$. This is then fused with the current-step IMU-based velocity $\mathbf{V}_{t+1}^{\mathrm{IMU}}$ into a temporary random variable $\mathbf{W}_{t+1}$. Assuming independence of the involved random variables,

$$\mathbf{W}_{t+1} \sim \mathcal{N}\left(\boldsymbol{\mu}_{\mathbf{W}_{t+1}}, \boldsymbol{\Sigma}_{\mathbf{W}_{t+1}}\right),$$

where

$$\boldsymbol{\Sigma}_{\mathbf{W}_{t+1}} = \mathrm{Cov}[\mathbf{W}_{t+1}] = \left(\boldsymbol{\Sigma}^{-1}_{\bar{\mathbf{V}}_{t+1}} + \boldsymbol{\Sigma}^{-1}_{\mathbf{V}^{\mathrm{IMU}}_{t+1}}\right)^{-1},$$
$$\boldsymbol{\mu}_{\mathbf{W}_{t+1}} = \mathbb{E}[\mathbf{W}_{t+1}] = \boldsymbol{\Sigma}_{\mathbf{W}_{t+1}} \left(\boldsymbol{\Sigma}^{-1}_{\bar{\mathbf{V}}_{t+1}} \boldsymbol{\mu}_{\bar{\mathbf{V}}_t t+1} + \boldsymbol{\Sigma}^{-1}_{\mathbf{V}^{\mathrm{IMU}}_{t+1}} \boldsymbol{\mu}_{\mathbf{V}^{\mathrm{IMU}}_{t+1}}\right).$$

Step 3.3: (*Final velocity correction*) The temporary random variable $\mathbf{W}_{t+1}$ is fused with information provided by the time derivative G_{t+1} of the magnetic field into the final velocity $\mathbf{V}_{t+1}$. The time derivative of the magnetic field is modeled as an independent 1D Gaussian random variable, $G_{t+1} \sim \mathcal{N}(g_{t+1}, \sigma^2_{\mathrm{G}})$, and estimated in flight using magnetometric measurements. The final velocity $\mathbf{V}_{t+1}$ is then normally distributed,

$$\mathbf{V}_{t+1} \sim \mathcal{N}\left(\boldsymbol{\mu}_{\mathbf{V}_{t+1}}, \boldsymbol{\Sigma}_{\mathbf{V}_{t+1}}\right),$$

and

$$\boldsymbol{\Sigma}_{\mathbf{V}_{t+1}} = \mathrm{Cov}[\mathbf{V}_{t+1}] = \left(\boldsymbol{\Sigma}^{-1}_{\mathbf{W}_{t+1}} + \frac{\nabla M(\mathbf{x}_{t+1}) \left(\nabla M(\mathbf{x}_{t+1})\right)^{\mathrm{T}}}{\sigma^2_{\mathrm{G}}}\right)^{-1}, \tag{2}$$

$$\boldsymbol{\mu}_{\mathbf{V}_{t+1}} = \mathbb{E}[\mathbf{V}_{t+1}] = \boldsymbol{\mu}_{\mathbf{W}_{t+1}} + \frac{g_{t+1} - \boldsymbol{\mu}^{\mathrm{T}}_{\mathbf{W}_{t+1}} \nabla M(\mathbf{x}_{t+1})}{\sigma^2_{\mathrm{G}}} \boldsymbol{\Sigma}_{\mathbf{V}_{t+1}} \nabla M(\mathbf{x}_{t+1}), \tag{3}$$

where $\mathbf{x}_{t+1}$ denotes the particle location updated in Step 3.1 and $M(\cdot)$ is the magnetic anomaly map.

The output from Step 3 consist of the updated position $\mathbf{x}_{t+1}$ and the corrected velocity $\mathbf{V}_{t+1}$.

4 Field validation

4.1 UAV platform

The proposed method was tested a VTOL (Vertical Take-Off and Landing) aircraft shown in Fig. 2. The UAV was equipped with a magnetometer system with high-precision scalar cesium units (Geometrics MFAM). To ensure reliable magnetic field measurements and mitigate disturbances, the system had to be calibrated to take into account two factors:

1. Aircraft orientation. First, ground-based measurements with a non-magnetic tripod were collected. Then, an artificial neural network was employed to approximate the disturbance in function of yaw, pitch, and roll angles. Finally, the disturbances estimated this way were subtracted in flight from the magnetic field measurements.

2. Solar activity. An additional ground magnetometer was employed to monitor solar activity and account for the associated fluctuations of the magnetic field.

Figure 2: VTOL aircraft used for validation. The magnetometer system was installed on the nose.

4.2 Magnetic map generation

After calibration, the magnetometer system was used to map the area extending between longitudes 16.64–16.69 deg and latitudes 54.565–54.586 deg. Carefully designed flight paths were used to ensure complete coverage of the area, the desired resolution and precision. The resulting magnetic map (Fig. 3) was generated using Bayesian regression, as described in [10]. The discrepancy between the collected magnetic measurements and the map was 0.12 nT on average.

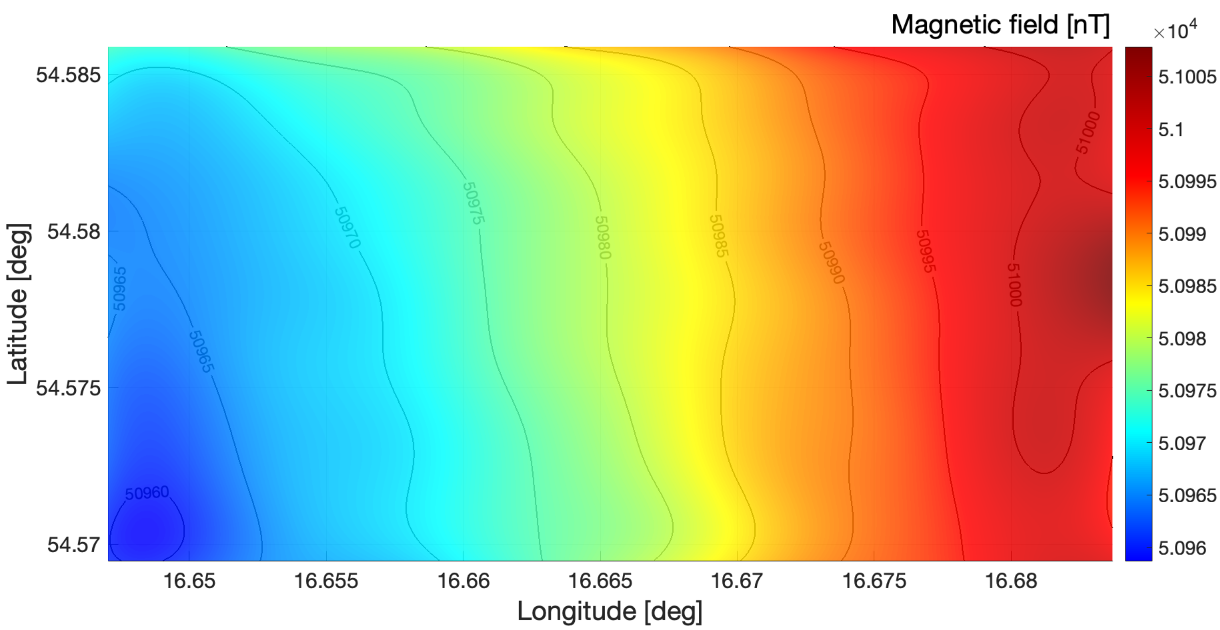

Figure 3: Map of the magnetic field generated using the collected measurements and Bayesian regression.

4.3 Test flight trajectory and Particle Filter procedure

The test flight trajectory, shown in yellow in Fig. 6, was defined using a number waypoints. The total duration of the test flight was 500 s. The IMU-based results included a deterministic velocity drift, which linearly increased with time and resulted at the end of the flight in the position error of 417.7 m. The Particle Filter procedure was started at $t = 50$ s. The initial number of particles was 100, and they were normally distributed around the estimated initial position with the standard deviation of 10^{-4} deg. The Particle Filter calculations were repeated every second, so that the time step $\Delta t = 1$ s.

Step 1: In each update $t \geq 50$, the weights were computed in Step 1 of the Particle Filter procedure by means of a Gaussian function with its argument being the difference between the measured magnetic reading o_t and the value read from the magnetic field map at the particle's location.

Step 2: During the resampling process in Step 2, particles with their normalized weights below 0.9 were discarded. New particles were then generated by sampling from a Gaussian distribution centered around the remaining particles with the standard deviation equal to $3 \cdot 10^{-5}$ deg. Throughout all time steps, the total number of particles, initially equal to 100, was kept between 50 and 200.

Step 3: The time derivative of the magnetic field, used by Eq. (3) in Step 3.3 (velocity correction), was computed using the increment of the collected magnetic measurements: $g_{t+1} = (o_{t+1} - o_t)/\Delta t$. The standard deviation σ_{G}, required in Eqs. (2) and (3)), represented the estimation error of the time derivative g_{t+1}. Its value was selected to correspond to the magnetic field measurement error, so that $\sigma_{\mathrm{G}}^2 = 0.5$ nT^2/s^2.

4.4 Results and discussion

For a comprehensive evaluation of positioning accuracy, the Particle Filter procedure was used both with and without the proposed velocity correction (that is, using only the uncorrected IMU-based velocity or correcting it using magnetometric measurements). In each case, a total of 100 test trajectories were computed. The resulting accuracies are plotted in Fig. 4 (for the uncorrected IMU-based velocity) and in Fig. 5 (for the corrected velocity).

In the initial phase of the flight (for $t < 150$ s), the average positioning errors suggest similar performance for both methods, as the errors obtained for the uncorrected and corrected velocities are comparable. A more significant divergence occurs for $t > 250$ s, with the average positioning error for the uncorrected velocity increasing up to 80.7 m at $t = 486$ s. In contrast, implementation of the proposed velocity correction substantially reduces the average positioning error, which remains consistently below 20.0 m for $t > 215$ s. The maximum error in this case occurs at time $t = 212$ s and equals 30.3 m, which is 62.4% lower than the maximum error obtained using the uncorrected IMU-based velocity. Moreover, with the proposed velocity correction, the total variation in positioning error is significantly reduced. These conclusions are confirmed by the visual analysis of trajectories obtained with both positioning methods, see

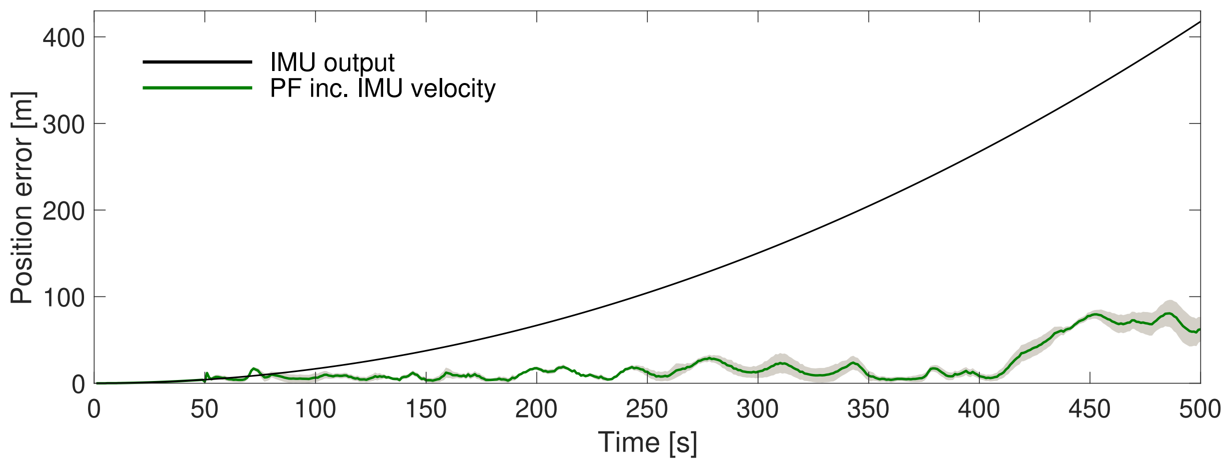

Figure 4: Positioning accuracy of Particle Filter using propagation model with uncorrected IMU-based velocity: mean position errors from 100 simulations (green line) with $\pm 1\sigma$ band (gray area). The reference (black line) corresponds to the position error obtained using inertial data only.

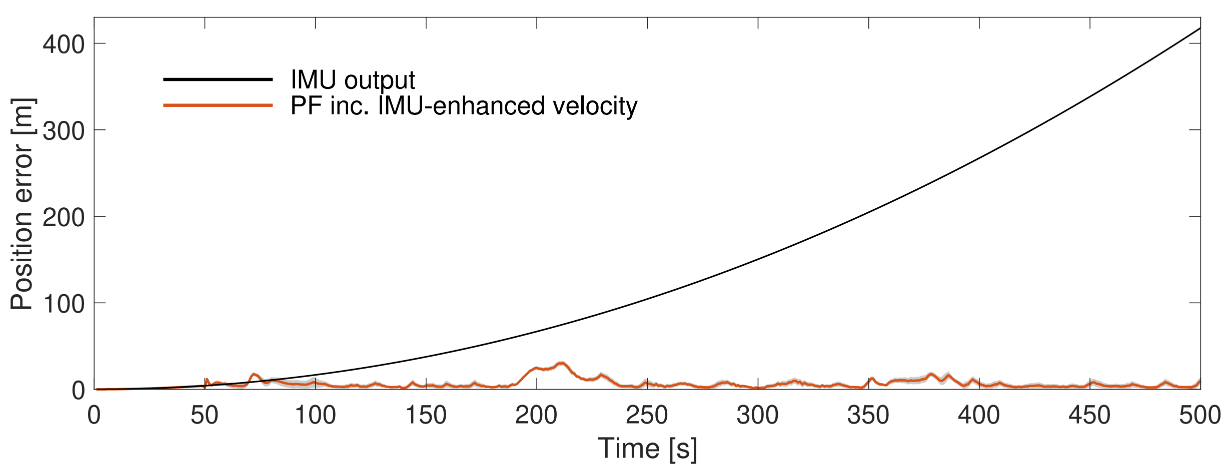

Figure 5: Positioning accuracy of Particle Filter using propagation model with corrected velocity (proposed fusion of inertial and magnetic measurements): mean position errors from 100 simulations (orange line) with $\pm 1\sigma$ band (gray area). The reference (black line) corresponds to the position error obtained using inertial data only.

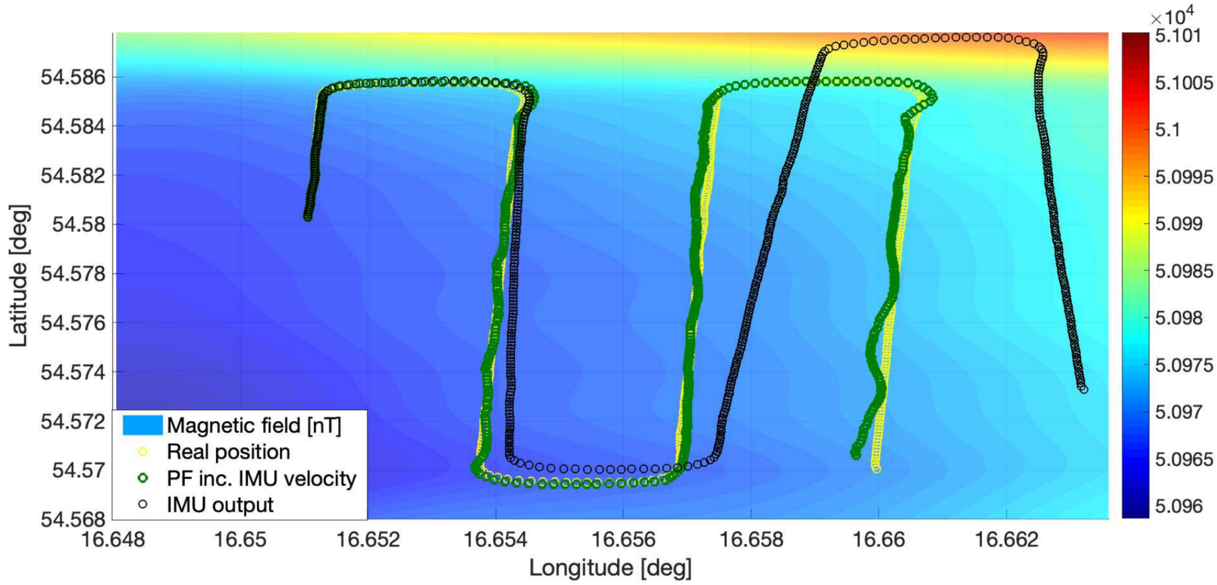

Figure 6: Trajectories obtained using the evaluated positioning methods. The trajectory shown for the Particle Filter with uncorrected IMU-based velocity is randomly selected from the 100 performed simulations.

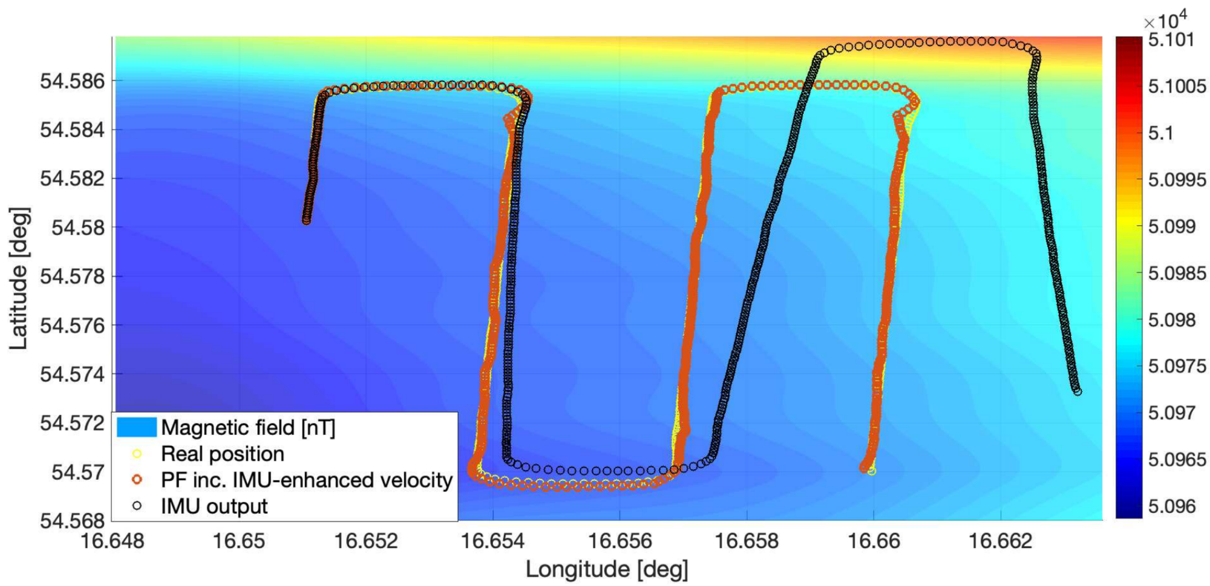

Figure 7: Trajectories obtained using the evaluated positioning methods. The trajectory shown for the Particle Filter with corrected IMU-based velocity (inertial/magnetic data fusion) is randomly selected from the 100 performed simulations.

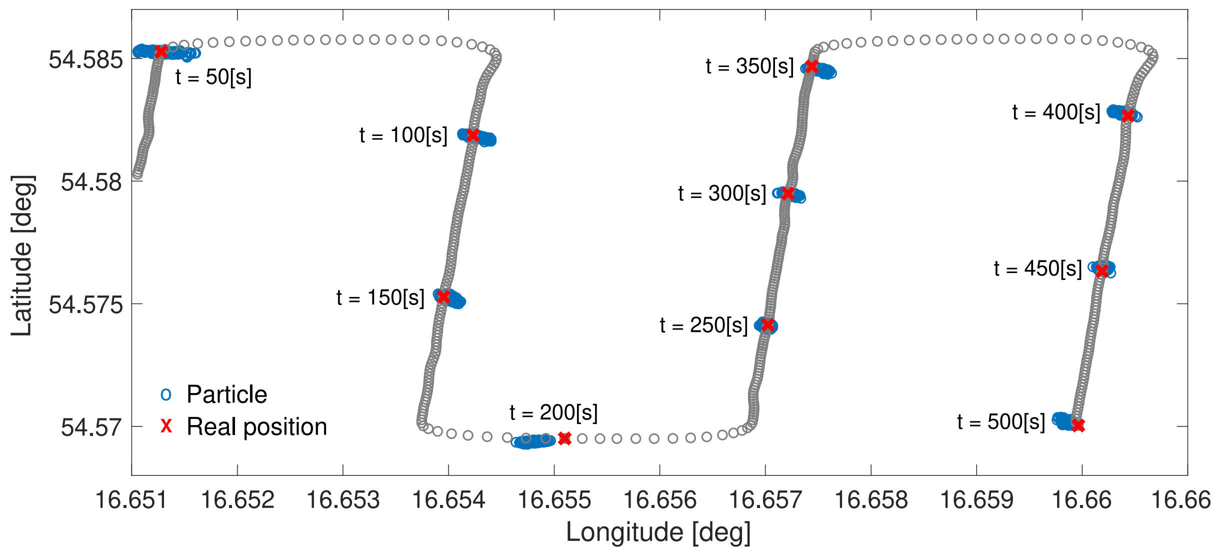

Figure 8: Particle distributions computed every 50 s by the Particle Filter with the corrected velocity (inertial/magnetic data fusion). The real reference trajectory is marked with gray circles. The red crosses indicate the actual UAV positions in the considered time steps. The particle distributions correspond to a simulation randomly selected from the set of 100 performed simulations.

Figs. 6 and 7. The evolution of particle distributions, sampled every 50 s, is illustrated in Fig. 8. These distributions are internally used by the Particle Filter procedure with the proposed inertial/magnetic data fusion and velocity correction. Their general characteristics stay consistent throughout the entire flight. As a result, the estimated position and UAV trajectory are smoother, which can be beneficial for the operation of the autopilot system.

5 Conclusion

This contribution presents an original method for UAV positioning in GNSS-denied environments. The approach is based on Particle Filter, and the measurements of the magnetic anomaly field are integrated at two stages. First, in the *propagation model stage*, velocity—typically derived from inertial measurements only—is additionally corrected using in-flight magnetometric measurements. This fusion of inertial and magnetic information is performed using the Bayesian formalism. Second, at the *position estimation stage*, the posterior distribution generated within the Particle Filter is computed by comparing magnetometric measurements with the magnetic field map, where the particles with the highest discrepancy are discarded.

The developed method was validated in a test flight using a VTOL-type UAV platform equipped with high-precision cesium magnetometers. In comparison to a typical approach based on IMU-only velocity, the proposed data fusion and velocity correction significantly reduced positioning errors and resulted in a smoother and more accurate estimated trajectory.

Acknowledgements

This research was funded by the National Centre for Research and Development (NCBR), Poland, under the grant agreement DOB-SZAFIR/01/B/018/04/2021.

REFERENCES

[1] Y. Lu, Z. Xue, G. S. Xia, and L. Zhang, "A survey on vision-based UAV navigation," *Geo-Spatial Information*, vol. 21, no. 1, pp. 21–32, 2018.

[2] A. V. R. Katkuri, H. Madan, N. Khatri, A. S. H. Abdul-Qawy, and K. S. Patnaik, "Autonomous UAV navigation using deep learning-based computer vision frameworks: A systematic literature review," *Array*, vol. 23, p. 100361, 2024.

[3] C. Zhu, M. Meurer, and C. Günther, "Integrity of visual navigation—developments, challenges, and prospects," *NAVIGATION: Journal of the Institute of Navigation*, vol. 69, no. 2, p. navi.518, 2022.

[4] G. Ouyang and K. Abed-Meraim, "A survey of magnetic-field-based indoor localization," *Electronics*, vol. 11, no. 6, p. 864, 2022.

[5] X. Wang, C. Zhang, F. Liu, Y. Dong, and X. Xu, "Exponentially weighted particle filter for simultaneous localization and mapping based on magnetic field measurements," *IEEE Transactions on Instrumentation and Measurement*, vol. 66, no. 7, pp. 1658–1667, 2017.

[6] J. Aulinas, Y. R. Pétillot, J. Salvi, and X. Lladó, "The SLAM problem: a survey," in *Artificial Intelligence Research and Development*, ser. Frontiers in Artificial Intelligence and Applications. IOS Press, 2008, vol. 184, pp. 363–371.

[7] M. Zmitri, H. Fourati, and C. Prieur, "Magnetic field gradient-based EKF for velocity estimation in indoor navigation," *Sensors*, vol. 20, p. 5726, 2020.

[8] V. F., R. Helmons, and M. Kok, "An extended kalman filter for magnetic field SLAM using Gaussian process regression," *Sensors*, vol. 22, p. 2833, 2022.

[9] Y. H. Kim, H. J. Kim, J. H. Lee, S. H. Kang, E. J. Kim, and J. W. Song, "Sequential batch fusion magnetic anomaly navigation for a low-cost indoor mobile robot," *Measurement*, vol. 213, p. 112706, 2023.

[10] Ł.. Jankowski, D. Pisarski, R. Konowrocki, B. Popławski, and R. Faraj, "Efficient real-time positioning using Bayesian analysis and magnetic anomaly field," *Measurement*, vol. 233, p. 114738, 2024.

[11] A. Canciani and J. Raquet, "Absolute positioning using the Earth's magnetic anomaly field," *NAVIGATION: Journal of the Institute of Navigation*, vol. 63, no. 2, pp. 111–126, 2016.

[12] A. Canciani and J. Raquet, “Airborne magnetic anomaly navigation,” *IEEE Transactions on Aerospace and Electronic Systems*, vol. 53, no. 1, pp. 67–80, 2017.

[13] T. N. Lee and A. J. Canciani, “MagSLAM: Aerial simultaneous localization and mapping using Earth’s magnetic anomaly field,” *Navigation*, vol. 67, no. 1, pp. 95–107, 2020.

[14] A. Gnadt, *Machine Learning-Enhanced Magnetic Calibration for Airborne Magnetic Anomaly Navigation*, San Diego, CA, USA, January 2022.